

Supplementary Materials of position-dependent partial convolutions for supervised spatial interpolation

Hirotaka Hachiya

HHACHIYA@WAKAYAMA-U.AC.JP

Graduate School of Systems Engineering, Wakayama University/Center for AIP, RIKEN

Kotaro Nagayoshi

NAGAYOSHI.KOTARO@G.WAKAYAMA-U.JP

Graduate School of Systems Engineering, Wakayama University/Center for AIP, RIKEN

Asako Iwaki

IWAKI@BOSAI.GO.JP

National Research Institute for Earth Science and Disaster Resilience

Takahiro Maeda

TMAEDA@BOSAI.GO.JP

National Research Institute for Earth Science and Disaster Resilience

Naonori Ueda

NAONORI.UEDA@RIKEN.JP

Center for AIP, RIKEN

Hiroyuki Fujiwara

FUJIWARA@BOSAI.GO.JP

National Research Institute for Earth Science and Disaster Resilience

Editors: Emtilay Khan and Mehmet Gönen

1. Additional information of classical spatial interpolation methods

Triangles used in classical interpolation methods, e.g., IDW and Kriging, are generated by Delaunay triangulation, as shown in Fig. 1.

2. Additional information of ground-motion data

Ground-motion simulation is a numerical computation (finite-difference) of seismic wave propagation from the earthquake source to the ground surface within a 3-D medium, as shown in the schematic drawing in Fig. 2.

3. Additional examples of spatial interpolation in motion data

Fig. 3, Fig. 5 and Fig. 7 depict examples of masked image $Y \odot M$, true image Y , and interpolated image \hat{Y} . In addition, Fig. 4, Fig. 6 and Fig. 8 depict true vs. predicted values. Figures show that given extremely sparse observed values (b), our proposed method, PoDIM (f), can produce fine-grained interpolated images which look much similar to the true one (a) and have higher PSNR scores than existing methods.

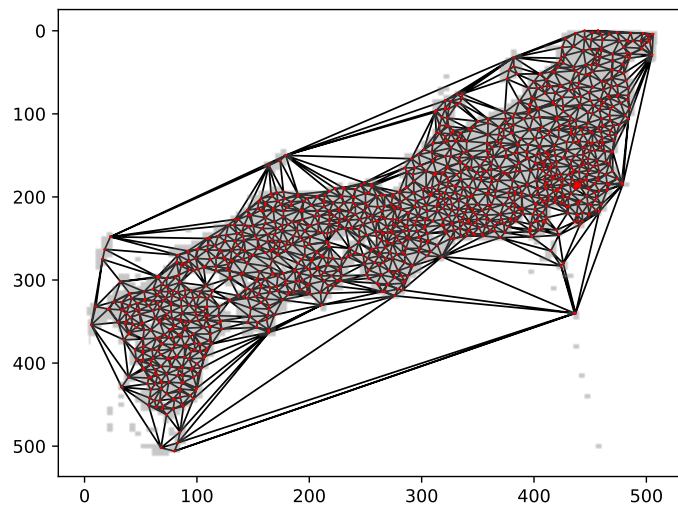


Figure 1: Delaunay triangulation split using `scipy.spatial.Delaunay` for strong motion stations K-NET and KiK-net in Fig. 1(a) subfigure (a).

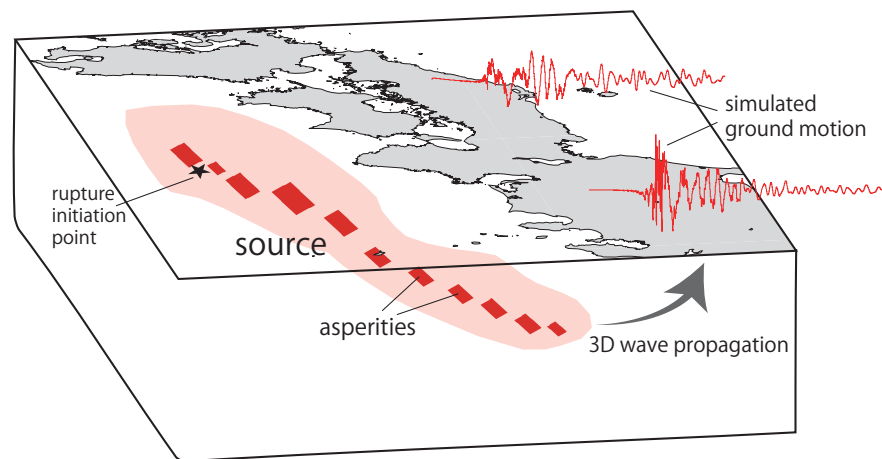


Figure 2: Schematic drawing of 3-D earthquake ground-motion simulation. The configuration of the earthquake source drawn on the map is exaggerated to improve visibility.

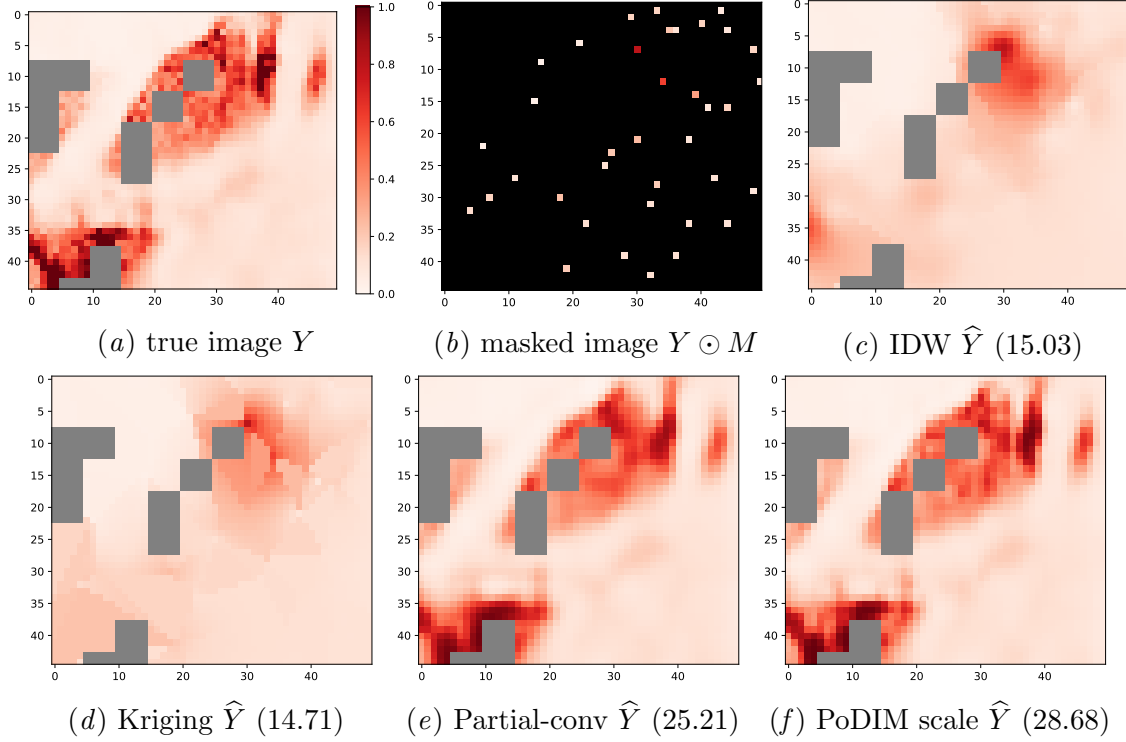


Figure 3: Examples of an enlarged version of Fig. 7 for Osaka region in Japan with the longitude from 134.93 to 136.03 and the latitude from 34.05 to 34.87.

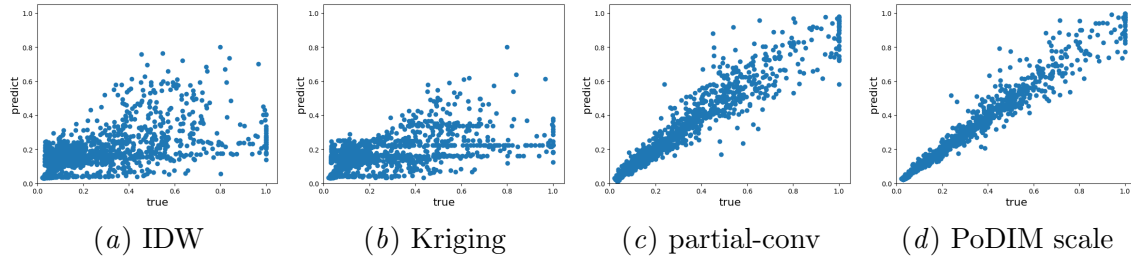


Figure 4: True vs. predicted values for Fig. 3.

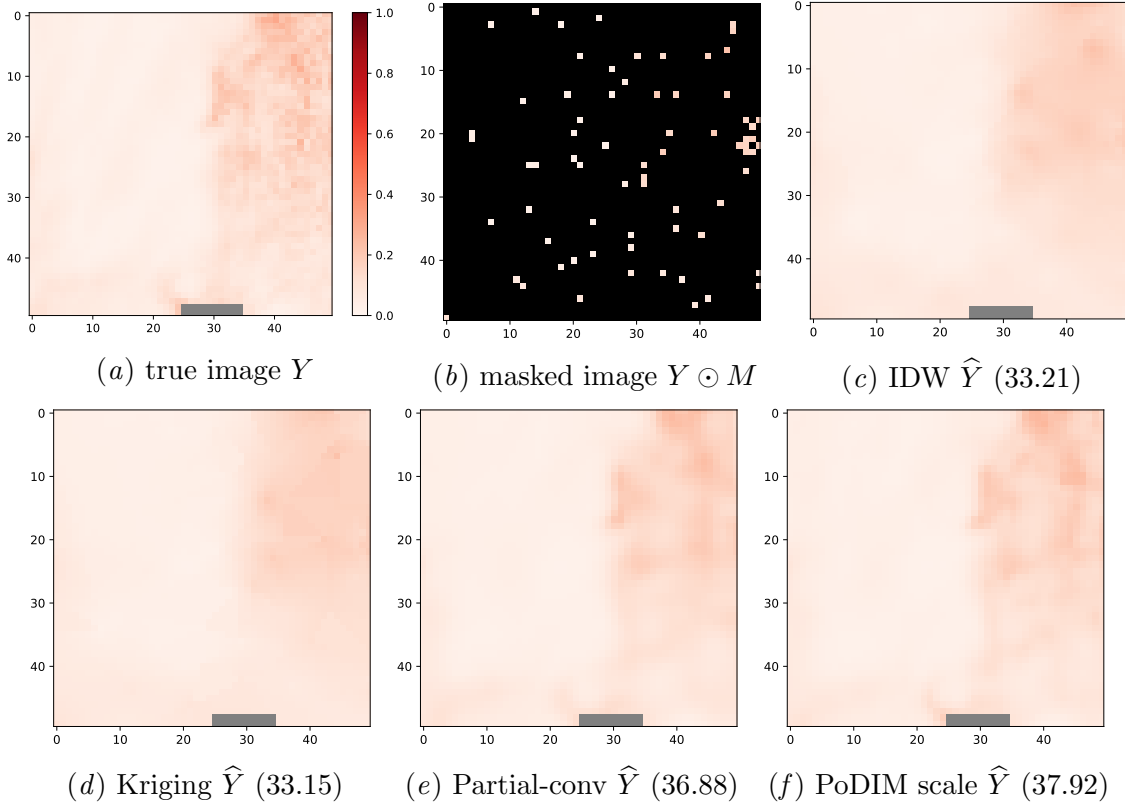


Figure 5: Examples of enlarged version of Fig. 7 in the manuscript for Tokyo region in Japan.

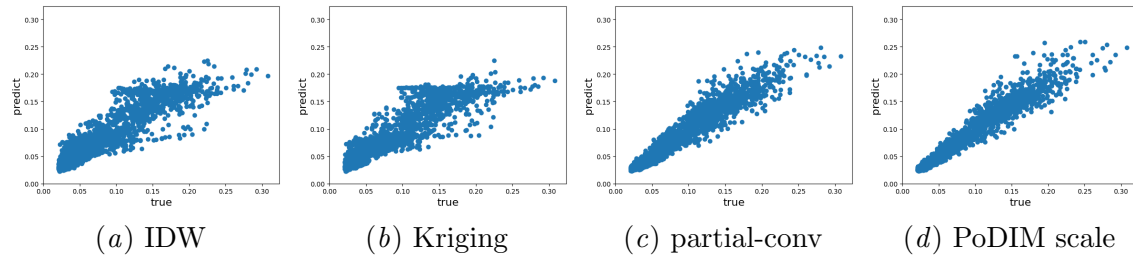


Figure 6: True vs. predicted values for Fig. 5.

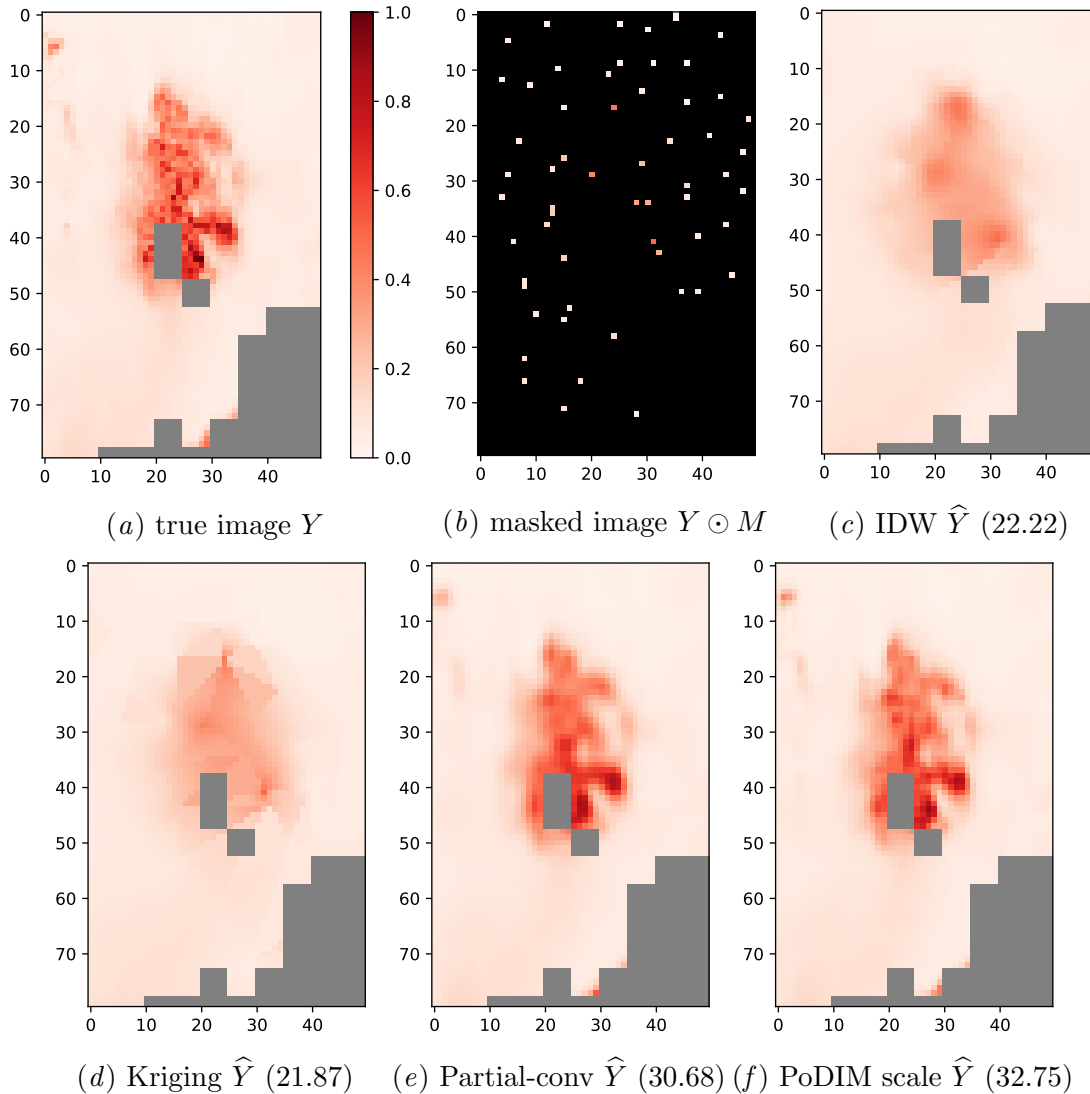


Figure 7: Examples of enlarged version of Fig. 7 in the manuscript for Nagoya region in Japan

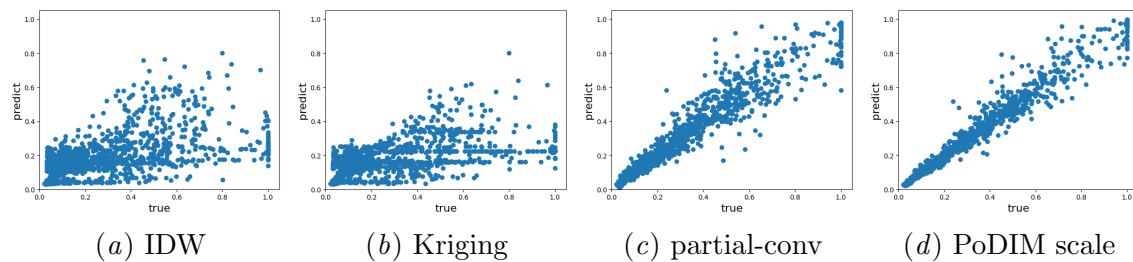


Figure 8: True vs. predicted values for Fig. 7.